Coexistence of Alternating Ferromagnetic and Antiferromagnetic Intermolecular Interactions in Organic Compounds. Synthesis, Structure, Thermal Stability, and Magnetic Properties of 2,4-Hexadiynylenedioxybis[2-(*p*-phenylene)-4,4,5,5-tetramethyl-4,5-dihydro-1*H*-imidazol-1-oxyl] Diradical[1]

Esteve Hernàndez-Gasio,[†] Montserrat Mas,[†] Elíes Molins,[†] Concepció Rovira,[†] Jaume Veciana,*[,†] Juan J. Borrás-Almenar,[‡] and Eugenio Coronado*[,‡]

Institut de Ciéncia dels Materials de Barcelona (CSIC), Campus de la U.A.B., 08193-Bellaterra, Barcelona, Spain, and Departamento de Química Inorgánica, Facultad de Química, Universidad de Valencia, C/Dr. Moliner 50, 46100-Burjasot, Valencia, Spain

Received July 18, 1994[⊗]

A crystalline phase of the 2,4-hexadiynylenedioxybis[2-(*p*-phenylene)-4,4,5,5-tetramethyl-4,5-dihydro-1*H*-imidazol-1-oxyl] diradical, **1**, has been prepared and characterized by X-ray diffraction, IR, UV-vis, and EPR spectroscopies, and magnetic susceptibility measurements. This phase belongs to the *C2/c* space group [a = 16.57(2) Å, b = 16.116(2) Å, c = 13.10(1) Å, β = 123.05(4)°, V = 2931(4) Å^3, Z = 4, d_{calc} = 1.30 g cm^{-3}, T = 21 °C, R_u = 0.092, R_w = 0.116]. The molecular structure of the diradical is characterized by an asymmetrical Z-shaped conformation. The most relevant features observed in the molecular packing are the large interdiacetylene separations—the shortest one is 8.285 Å—and the alternation in the characteristics of the intermolecular contacts between the radical side groups of the DA; which are joined by hydrogen bonds between the oxygen atoms of NO groups and aromatic hydrogen atoms. On the basis of accepted structural criteria, this solid-state structure should not support a single-crystal topochemical polymerization and, accordingly, the UV-induced polymerization was not achieved. Thermal treatment, however, turns the crystals from blue to dark brown. Thermal analyses under nitrogen, performed with DSC and TGA techniques, reveal an explosive and complex decomposition, at temperatures higher than 90 °C, with an evolution of gaseous NO (GC-MS) and a destruction of most of the radical centers of diradical molecules, as demonstrated by EPR and magnetic measurements. The study of the temperature dependence of the EPR signals of very diluted solutions of diradical **1** shows that it has a thermally modulated intramolecular exchange interaction due to the flexibility of the spacers joining the two radical centers and, furthermore, that when this diradical adopts a rigid conformation the two radical moieties are magnetically isolated ($J^{intra}/k \sim 0$ K). EPR studies on polycrystalline samples of diradical **1** provide evidences for significant intermolecular exchange couplings between radical side groups of neighbor diradicals. The magnetic susceptibility of **1** suggests the simultaneous presence of dominant antiferromagnetic interactions together with very weak ferromagnetic ones; in agreement with the observed alternation of structural characteristics and the solid state EPR spectrum. This magnetic behavior is quantitatively described by a linear Heisenberg chain of $S = {}^1/_2$ spins with alternating F-AF intermolecular interactions of $J_{AF}{}^{inter}/k = -3.9$ K and $J_F{}^{inter}/k \sim +1.2$ K. The presence of ferromagnetic interactions in **1** is attributed to the substituted diacetylenic unit, which, by structural reasons, obstructs the natural tendency of radical centers to interact only in an antiferromagnetic fashion. Finally, a reinterpretation of the magnetic data of other related organic compounds showing alternating F-AF interactions is presented, and the resulting exchange parameters correlated with the structural features of the solids.

Introduction

The quest for molecular-based ferromagnets having transition metals as spin carrier centers has culminated with the characterization of some examples of this kind of magnetic materials.[2] The search for purely organic ferromagnetic materials, however, continues to be of

[†] Institut de Ciència de Materials de Barcelona (CSIC).
[‡] Universidad de Valencia.
[⊗] Abstract published in *Advance ACS Abstracts,* October 15, 1994.

(1) Preliminary reports of parts of this work have been presented in the following: (a) Hernàndez, E.; Galán, A.; Rovira, C.; Veciana, J.; Mas, M.; Molins E.; Miravitlles, C. *Proceedings of the International Conference on Science and Technology of Synthetic Metals* (ICSM '92); Statröm, S., Salaneck, W. R., Inganäs, O., Hjertberg, T., Eds. *Synth. Met.* **1993**, *55-57*, 761-766. (b) Veciana, J.; Rovira, C.; Hernàndez, E.; Molins, E.; Mas, M. *Proceedings of the International Symposium on Chemistry and Physics of Molecular Based Magnetic Materials*; Iwamura, H., Miller, J. S., Eds. *Mol. Cryst. Liq. Cryst.* **1993**, *232-233*, 163-172.

0897-4756/94/2806-2398$04.50/0

interest. Two major approaches are being used in the design and synthesis of elusive purely organic magnets; namely, *intermolecular* and *intramolecular spin alignment* approaches. Up to now, only the first approach has produced a few molecular-based materials with bulk ferromagnetic behaviors.[3] Reports of ferromagnetic polymeric materials with the second approach have been plagued by ill-defined compositions, low yields, lack of characterizations, and poor reproducibilities;[4,5] and when some of these materials have been obtained again, the cooperative magnetic property has not been reproduced.[6] Thus, the obtention of a polymeric ferromagnet continues to be a challenge.

The design of a crystalline molecular solid showing ferromagnetic interactions between the spins belonging to neighboring molecules is hampered by the intrinsic difficulty that exists for predicting the crystal structure of an organic molecular solid.[1,2] To overcome this difficulty, *crystal engineering tools*, sometimes named as *crystalline design elements*, are needed. Such tools would, in principle, allow us to control the crystal lattice of the molecular solid and therefore the involved intermolecular magnetic interactions. In this context it appeared to us that diacetylenes (DAs) and polydiacetylenes (PDAs) would provide such types of crystal engineering tools.[1] In fact, PDAs can be obtained, via a solid-state reaction from the corresponding DAs, as planar and fully conjugated polymer chains extending along a given crystallographic direction.[7] In addition, both the PDAs and the DAs usually show a high degree of ordering both in the polymeric backbone as in the diacetylenic units and in their side groups. Therefore, PDAs and DAs having free radicals as side groups would permit us to show how the structural constraints, imposed by either the polymeric backbone or the diacetylenic unit, affect both the packing pattern and the through-space magnetic interactions between the radical centers. Moreover, the structural constraints imposed by these crystal engineering tools would in principle restrict the degrees of freedom for the packing of radical side groups, obstructing in such a way the natural tendency of radicals centers to interact antiferromagnetically. Thus, the obtention and study of polyradical PDAs would provide clues that could be useful for the preparation of a bulk polymeric ferromagnet.

Herein we report the obtention and the detailed structure and magnetic and thermal properties of a crystalline phase of a DA having α-nitronyl nitroxide radicals as side groups, i.e., the 2,4-hexadiynylenedioxybis[2-(*p*-phenylene)-4,4,5,5-tetramethyl-4,5-dihydro-1*H*-imidazol-1-oxyl] diradical (**1**). The magnetic properties of this crystalline phase are discussed using a chain model which assumes the coexistence of alternating ferromagnetic and antiferromagnetic intermolecular interactions and correlated with the structural characteristics of the material. In addition, a magneto-structural comparison of this system with other purely organic magnetic materials which have also shown evidence of having opposed magnetic interactions is also reported. Finally, the structural and magnetic characterization of the product(s) derived from the thermal treatment of the diradical **1** are also presented.

At the same time that the present work was in course and some preliminary results were presented,[1] Zhang et al. communicated a couple of brief reports about the same diradical.[8] They claimed that diradical **1** shows at 1.5 K a bulk ferromagnetic behavior, and it undergoes, without polymerizing, a phase transition at 87 °C, giving rise to a material that exhibits antiferromagnetic interactions.[8b,c] These authors also claimed that this diradical can be polymerized by heating under vacuum and the resulting polyradical PDA shows a weak ferromagnetism.[8a] All these remarkable results increased even more our interest for polyradical PDAs,[1,9] promoting a detailed and careful magneto-structural study of the diacetylenic diradical **1** as well as of its thermally produced derivative(s), which is set forth in the following.

Results and Discussion

Synthesis. The preparation of diradical **1** was performed using a synthetic sequence, which is outlined in Scheme 1, different from that used for Zhang et al.[8a] Thus, the monoacetylenic radical **2** was obtained by a nucleophilic substitution on the *p*-toluenesulfonate of 2-propynyl using an excess of the phenoxide derived from the radical phenol **3**.[10] Such a radical phenoxide was generated in situ, from the corresponding phenol **3**, with an excess of potassium *tert*-butoxide (*t*-BuOK) in tetrahydrofuran (THF). The oxidative coupling of the

(2) For a recent overview on this topic, see: (a) *Proceedings of the Symposium on Ferromagnetic and High-Spin Molecular Based Materials*; 197th National Meeting of the American Chemical Society, Dallas, TX, April 1989; American Chemical Society: Washington, DC. Miller, J. S., Dougherty, D. A., Eds. *Mol. Cryst. Liq. Cryst.* **1989**, *176*, 1–562. (b) Materials Research Society Symposium Proceedings, 175; Chiang, L. Y., Chaikin, P. M., Cowan, D. O., Eds. *Advanced Organic Solid State Materials* **1989**, 3–92. (c) Gatteschi, D., Kahn, O., Miller, J. S., Palacio, F., Eds. *Molecular Magnetic Materials*; Kluwer Academic: Dordrecht, 1991. (d) Proceedings of International Symposium on Chemistry and Physics of Molecular Based Magnetic Materials Tokyo, Japan, 25–30 Oct 1992. *Mol. Cryst. Liq. Cryst.* **1993**, *232–233*.

(3) (a) Tamura, H.; Nakazawa, Y.; Shiomi, D.; Nozawa, K.; Hosokoshi, Y.; Ishikawa, M.; Takahashi, M.; Kinoshita, M. *Chem. Phys. Lett.* **1991**, *186*, 401. (b) Chiarelli, R.; Rassat, A.; Rey, P. *J. Chem. Soc., Chem. Commun.* **1992**, 1081. Rassat, A. In ref 1d. (c) Allemand, P.-M.; Khemani, K. C.; Koch, A.; Wudl, F.; Holczer, K.; Donovan, S.; Grüner, G.; Thompson, J. D. *Science* **1991**, *253*, 301.

(4) Torrance, J. B.; Oostra, S.; Nazzal, A. *Synth. Met.* **1987**, *19*, 708. Torrance, J. B.; Bagus, P. S.; Johannsen, I.; Nazzal, A.; Parkin, S. S. P.; Batail, P. *J. Appl. Phys.* **1988**, *63*, 2962–2965.

(5) Korshak, Yu. V.; Ovchinnikov, A. A.; Shapiro, A. M.; Medvedeva, T. V.; Spector, V. N. *Pisma Zh. Eksp. Teor. Fiz.* **1986**, *63*, 309–311. Korshak, Yu. V.; Medvedeva, T. V.; Ovchinnikov, A. A.; Spector, V. N. *Nature* **1987**, *326*, 370–372. Buchachenko, A. L.; Shibaeva, R. P.; Rozenberg, L. P.; Ovchinnikov, A. A. *Khim. Phys.* **1987**, *6*, 773–778. Cao, Y.; Wang, P.; Hu, Z.; Ki, S.; Zhang, L.; Zhao, J. *Solid State Commun.* **1988**, *68*, 817; *Synth. Met.* **1988**, *27*, B265.

(6) Miller, J. S.; Epstein, A. J.; Glatzhofer, D. T.; Calabresse, J. C. *J. Chem. Soc., Chem. Commun.* **1988**, 322. Miller, J. S.; Glatzhofer, D. T.; Laversanne, R.; Brill, T. B.; Tinken, M. D.; O'Connor, C. J.; Zhang, J. H.; Calabresse, J. C.; Epstein, A. J.; Chittipeddi, S.; Vaca, P. *Chem. Mater.* **1990**, *2*, 60–69.

(7) (a) Wegner, G. *Z. Naturforsch.* **1969**, *24*, 824. (b) Baughman, R. H. *J. Polym. Sci., Polym. Phys. Ed.* **1974**, *12*, 1511. (c) Bloor, D. In *Polydiacetylenes*; Bloor, D., Chance, R. R., Eds. *NATO ASI, Ser. E, No. 102*; Martinus Nijhoff Publishers: Dordrecht, 1985; p 15. (d) Baughmann, R. H. *Ann. N. Y. Acad. Sci.* **1978**, *313*, 705–725. (e) Enkelmann, V. *Adv. Polym. Sci.* **1984**, *63*, 91. (f) Bassler, H. *Ibid.* **1984**, *63*, 48.

(8) (a) Zhang, D.; Wu, P.; Zhu, D.; Zhou, W. *Mater. Res. Soc. Proc.* **1992**, *247*, 443. (b) Zhang, D.; Zhou, W.; Zhu, D. Communication presented at the International Conference on Science and Technology of Synthetic Metals (ICSM '92), August, 1992, Göteborg, Sweden. (c) Zhang, D.; Zhou, W.; Zhu, D. *Solid State Commun.* **1993**, *86*, 291–294.

(9) (a) Veciana, J.; Galan, A.; Riaza, J.; Armet, O.; Molins, E.; Miravitlles, C. *Mol. Cryst. Liq. Cryst.* **1988**, *156*, 289. (b) Hernàndez, E.; Galan, A.; Rovira, C.; Veciana, J. *Synthesis* **1992**, 1164.

(10) Ullman, E. F.; Osiecki, J. H.; Boocock, D. G. B.; Darcy, R. *J. Am. Chem. Soc.* **1972**, *94*, 7049.

Scheme 1

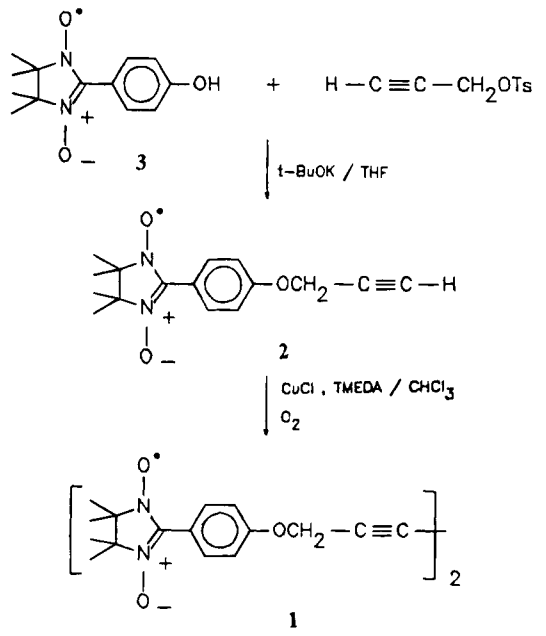

monoacetylenic radical **2** with oxygen, using copper(I) chloride/*N,N,N′,N′*-tetramethylethylenediamine (TMEDA) as a catalyst,[11] gave finally the diacetylenic diradical **1**.

Crystalline Structure. Deep blue parallelepipedic crystals of the diradical **1**, adequate for the X-ray crystal structure analysis, were obtained by slow evaporation at room temperature from a saturated chloroform solution containing this diradical. These crystals are the same crystalline phase as that previously reported for diradical **1**, despite their apparently distinct crystallographic parameters. In fact, the crystal cell referenced by Zhang et al. belongs to the space group *I2/a*,[8a] which can be converted to the standard group *C2/c* by the proper transformation, obtaining in such a way cell parameters that are very close to those obtained by us.[12] Since the crystalline structure of this diradical was only superficially communicated and some relevant aspects were misunderstood, a brief description of the most interesting details are here presented; in order to reinterpret and discuss the physicochemical properties of **1**.

(a) Molecular Geometry. The molecular geometry of **1** in the crystal as well as the atom labeling for a half of the diradical molecule, the asymmetric unit, are shown in Figure 1. The fractional coordinates and isotropic thermal parameters are summarized in Table 1. Selected bond lengths and angles are given in Table 2. The diacetylenic moiety is linear and displays bond lengths typical of most diacetylenes (DAs):[7d] *d*(C17–C17*) = 1.360(2) Å, *d*(C17–C16) = 1.200(1) Å, *d*(C16–C15) = 1.460(1) Å. The five-membered ring has the usual slightly distorted planar structure; the atoms C11 and C12 being situated 0.265 Å above and 0.231 Å below, respectively, from the mean plane defined by the atoms O10, N9, C8, N13, O14. The bond lengths of the two unique N–O groups are equal, within the experimental error −1.288(7) Å (N9–O10) and 1.290(7) Å (N13–O14)− as also occurs with those of N–C(sp^2) bonds −1.350(9) Å (C8–N9) and 1.347(9) Å (C8–N13). Moreover, such distances are very close to those reported for other related α-nitronyl nitroxide radicals.[13] These results strongly suggest the equivalence of the two unique N–O groups due to the delocalization of the unpaired electron mainly on the O10–N9–C8–N13–O14 group.[14]

The geometry of the asymmetric unit can be properly described by the dihedral angles between the mean

Table 1. Fractional Coordinates (×10⁴) and Isotropic Thermal Parameters for Diradical 1

atom	*X*	*Y*	*Z*	B_{eq}
O1	10489(4)	2976(3)	4834(5)	5.81
O10	8552(5)	−653(3)	2706(5)	6.81
O14	7468(5)	1336(3)	−325(5)	6.87
N9	8122(5)	−281(4)	1667(5)	4.38
N13	7587(4)	645(4)	239(5)	4.08
C2	9933(5)	2339(4)	4110(6)	4.10
C3	10066(5)	1501(4)	4425(6)	4.55
C4	9474(5)	924(4)	3556(6)	4.28
C5	8763(4)	1153(4)	2375(5)	3.52
C6	8625(5)	1998(4)	2070(6)	3.89
C7	9218(5)	2578(4)	2946(6)	4.21
C8	8170(5)	530(4)	1451(6)	3.55
C11	7614(6)	−763(5)	524(7)	5.62
C111	7103(6)	−1495(5)	626(9)	6.21
C112	8372(7)	−1092(6)	305(9)	6.85
C12	6993(5)	−101(4)	−384(6)	4.79
C121	6790(9)	−151(6)	−1638(7)	8.36
C122	6050(6)	18(6)	−461(1)	8.79
C15	11172(6)	2785(6)	6084(7)	5.44
C16	10693(6)	2733(5)	6744(6)	4.50
C17	10251(6)	2740(4)	7226(6)	4.07

Table 2. Selected Bond Lengths (Å) and Angles (deg) for Diradical 1

C17–C17*	1.360(2)	C16–C15–O1	110.2(7)
C16–C17	1.200(1)	C15–O1–C2	116.7(6)
C15–C16	1.460(1)	O1–C2–C3	126.0(6)
O1–C15	1.430(1)	C2–C3–C4	118.9(6)
C1–C2	1.359(8)	C3–C4–C5	121.9(6)
C2–C3	1.393(7)	C4–C5–C8	121.2(6)
C3–C4	1.381(7)	C5–C8–N9	125.5(6)
C4–C5	1.389(7)	C8–N9–O10	127.6(6)
C5–C8	1.463(9)	C8–N13–O14	125.5(6)
C8–N9	1.350(9)	C8–N9–C11	111.3(6)
C8–N13	1.347(9)	N9–C11–C12	101.2(6)
N9–O10	1.288(7)		
N13–O14	1.290(7)		
N9–C11	1.476(9)		
N13–C12	1.484(9)		
C11–C12	1.510(1)		

(11) Hay, A. S. *J. Org. Chem.* **1962**, *27*, 3320.

(12) The spatial transformation of the space group *I2/a* to the *C2/c* one is given by the following matrix:

$$\begin{pmatrix} 1 & 0 & 1 \\ 0 & -1 & 0 \\ 0 & 0 & -1 \end{pmatrix}$$

(13) (a) Wong, W.; Watkins, S. F.; *J. Chem. Soc., Chem. Commun.* **1973**, 888. (b) Allemand, P.-M.; Fite, C.; Srdanov, G.; Keder, N.; Wudl, F.; Canfield, P. *Synth. Met.* **1991**, *41–43*, 3291. (c) Awaga, K.; Inabe, T.; Nagashima, U.; Maruyama, Y. *J. Chem. Soc., Chem. Commun.* **1989**, 1617; *corrigenda* **1990**, 520. (d) Turek, P.; Nozawa, K.; Shiomi, D.; Awaga, K.; Inabe, T.; Maruyama, Y.; Kinoshita, M. *Chem. Phys. Lett.* **1991**, *180*, 327. (e) Awaga, K.; Inabe, T.; Nagashima, U.; Nakamura, T.; Matsumoto, M.; Kamabata, Y.; Maruyama, Y. *Chem. Lett.* **1991**, 1777. (f) Awaga, K.; Inabe, T.; Maruyama, Y. *Chem. Phys. Lett.* **1992**, *190*, 349. (g) Awaga, K.; Inabe, T.; Maruyama, Y.; Nakamura, T.; Matsumoto, M. *Chem. Phys. Lett.* **1992**, *195*, 21. (h) Sugano, T.; Tamura, M.; Kinoshita, M.; Sakai, Y.; Ohashi, Y. *Chem. Phys. Lett.* **1992**, *200*, 235. (i) Shiomi, D.; Tamura, M.; Sawa, H.; Kato, R.; Kinoshita, M. *Synth. Met.* **1992**, *55–57*, 3279. (j) Alies, F.; Luneau, D.; Laugier, J.; Rey, P. *J. Phys. Chem.* **1993**, *97*, 2922.

(14) Additional evidence supporting this delocalization are found through the solution EPR spectra in the low-temperature limit and through semiempirical molecular orbital calculations (vide infra).

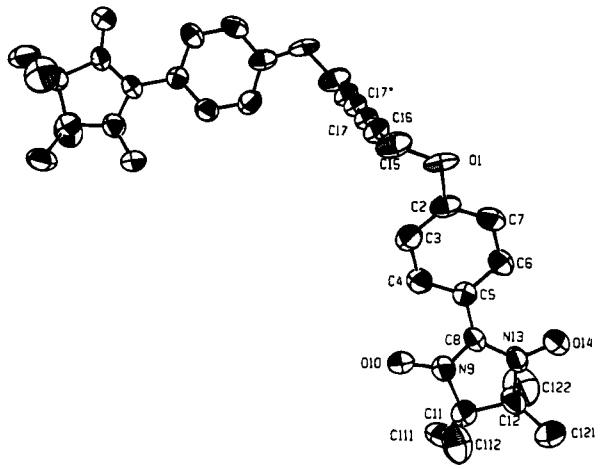

Figure 1. ORTEP view of the molecular geometry of diradical **1** in the crystal, showing the numbering of the atoms of the asymmetric unit. The two halves of the molecule are related by the symmetry operation $(2 - x, y, 1.5 - z)$.

planes defined by O10–N9–C8–N13–O14 (plane 1), C2–C3–C4–C5–C6–C7 (plane 2), and O1–C15–C16–C17 (plane 3) atoms. The corresponding values of such angles are 13° (plane 1–plane 2) and 82° (plane 2–plane 3). Thus, whereas the five-membered ring and the phenyl ring are almost coplanar, they are practically perpendicular to the plane defined by the atoms of the diacetylenic moiety and the CH_2O spacer. The resulting molecular geometry, as shown in Figure 1, closely resembles the Z-shaped geometry usually found in symmetrical DAs with $-CH_2O-$ and $-CH_2OSO_2-$ spacers and substituted phenyls as side groups.[15,16] Nevertheless, the two side groups in **1** molecules are not related by a crystallographic inversion center, contrary to the situation commonly found in Z-shaped DAs.[15] Instead, the two side groups are oriented so that their long axes are perpendicular to each other and to the diacetylenic moiety and, moreover, their two phenyl planes are almost parallel to each other as can be clearly visualized in Figure 1.

(b) Crystal Packing. A projection of the crystal structure on the *ac* crystallographic plane is shown in Figure 2. The packing pattern shows two outstanding features. First, the diacetylenic moieties are stacked along the three crystallographic axes and along the two diagonals of the *ab* plane. Along such stacks, the diacetylenic moieties are essentially parallel and the shortest distance observed between the centers of adjacent moieties is 8.285 Å. The large interdiacetylene separations contrasts strikingly with the nearest separation (3.75 Å) claimed by Zhang et al. for this compound.[8a] Actually, such a distance is not an interdiacetylenic one but the distance between C16 and C16′ atoms inside a diacetylenic group of a DA molecule. Thus, on the basis of the accepted structural criteria, *the observed interdiacetylene separations should not support the solid-state topochemical polymerization of this crystal phase of* **1**.[7] In fact, such a type of polymerizability is a common characteristic of those DAs having, among other structural prerequisites, close-packed (3.5–6.5 Å) diacetylenic moieties.[7] Second, the side groups of the diacetylenic moieties are stacked along the two diagonals of the *bc* plane. Along the stacks the side groups are arranged in side-by-side and head-to-tail fashions as is shown in Figure 3.

It is important to emphasize that the unique significant intermolecular short contacts (≤4 Å) present in the crystal structure are those displayed in Figure 3 as broken lines and, moreover, that in such short contacts always the oxygen atoms belonging to NO radical centers are involved. Thus, it seems that such oxygen atoms that are strongly polarized, $N^{\delta+}-O^{\delta-}$, supporting large negative charge densities ($\delta = -0.34$) as revealed by semiempirical MO (AM1) calculations, play an important role in the crystal packing of **1**. In particular, such atoms establish hydrogen bonds with the positively charged aromatic hydrogen atoms of the side groups belonging to neighbor molecules (see Table 3).[17]

The intermolecular contact distances relevant for the magneto-structural correlation of diradical **1** are also given in Table 3. As can be clearly seen by inspection of Figure 3 and Table 3, the intermolecular contacts established by each radical center and its two neighbors within the stacks are different. Consequently, *there is clearly an alternation in the characteristics of the intermolecular contacts along the stacks*. The side group belonging to the *i* molecules (see Figure 3 for the meaning of the symmetry codes *i*, *ii*, and *iii*) establishes two C6 (and H6)···O14 and two C7 (and H7)···O14 contacts with its symmetry-related neighbor molecules *ii*, but only one C3 (and H3)···O10 contact with the symmetry-related one *iii* is observed. Notice that the separations between C and O atoms are slightly higher than the sum of the van der Waals radii of the involved atoms. On the other hand, the separations between the two α-nitronyl nitroxide oxygen atoms are also remarkably different: 3.836 Å ($O14^{(i)}\cdots O14^{(ii)}$) and 5.666 Å ($O10^{(i)}\cdots O10^{(iii)}$). Both values are higher than the sum of the van der Waals radii of the oxygen atoms (3 Å). Finally, no intermolecular contacts shorter than 6 Å are observed between atoms belonging to neighboring stacks.

Solid-State Reactivity. With the purpose of validating experimentally the lack of polymerizability of **1**

(15) (a) Enkelmann, V.; Wegner, G. *Angew. Chem., Int. Ed. Engl.* **1977**, *16*, 6. (b) Morosin, M.; Harrah, L. *Acta Crystallogr. B* **1977**, *33*, 1760. (c) Mayerle, J. J.; Clarke, T. C. *Acta Crystallogr. B*, **1978**, *34*, 143. (d) Herbstein, F. H. *Acta Crystallogr. B*, **1979**, *35*, 1661. (e) Fischer, D. A.; Ando, D. J.; Bloor, D.; Hursthouse, M. B. *Acta Crystallogr. B* **1979**, *35*, 2075. (f) Williams, R. L.; Ando, D. J.; Bloor, D.; Hursthouse, M. B. *Acta Crystallogr. B*, **1979**, *35*, 2072. (g) Ando, D. J.; Bloor, D.; Hubble, C. L.; Williams, R. L.; *Makromol. Chem.* **1980**, *181*, 453. (h) McGhie, A. R.; Lipscomb, G. F.; Garito, A. F.; Desai, K. N.; Kalyanaraman, P. S. *Makromol. Chem.* **1981**, *182*, 965. (i) Williams, R. L.; Ando, D. J.; Bloor, D.; Hursthouse, M. B.; Montevalli, M. *Acta Crystallogr. B* **1982**, *38*, 2078. (j) Galiotis, C.; Young, R. J.; Ando, D. J.; Bloor, D. *Makromol. Chem.* **1983**, *184*, 1083. (k) Ando, D. J.; Bloor, D.; Hursthouse, M. B.; Montevalli, M. *Acta Crystallogr. C* **1985**, *41*, 224. (l) Ando, D. J.; Bloor, D.; Hursthouse, M. B.; Montevalli, M. *Acta Crystallogr. C*, **1985**, *41*, 227. (m) Ando, D. J.; Bloor, D.; Hursthouse, M. B.; Montevalli, M. *Acta Crystallogr. C* **1986**, *42*, 1049. (n) Ayme, J. P.; Schott, M.; Bertault, M.; Toupet, M. *Acta Crystallogr. B* **1988**, *44*, 617.

(16) A detailed revision of the crystal structures of symmetrical DAs using the Cambridge Structural Database, version 3.4 January 1989, allows one to determine that DAs with $-CH_2O-$ and $-CH_2SO_2-$ spacers and substituted phenyl side groups display only three molecular geometries, which, according to Bloor et al.[7c] have been called *linear*, *Z-shaped*, and *S-shaped*. The details of this study will be published in a forthcoming paper.

(17) It is worth noting that in between $C3^{(i)}$ [or $C6^{(ii)}$ and $C7^{(iii)}$] and $O10^{(iii)}$ [or $O14^{(i)}$] there is the $H3^{(i)}$ [or $H6^{(ii)}$ and $H7^{(iii)}$] hydrogen atom. Thus, it is possible to consider the existence of intermolecular contacts $C3-H3^{(i)}\cdots O10^{(iii)}$ [and $C6-H6^{(ii)}\cdots O14^{(i)}$ and $C7-H7^{(ii)}\cdots O14^{(i)}$]. These contacts fulfill all the geometrical requirements to be classified as C–H···O hydrogen bonds. See, for example: (a) Taylor, R.; Kennard, O. *Acc. Chem. Res.* **1984**, *17*, 320. (b) Desiraju, G. R. *Crystal Engineering: The Design of Organic Solids*; Elsevier: New York, 1989. (c) Desiraju, G. R. *Acc. Chem. Res.* **1991**, *24*, 290.

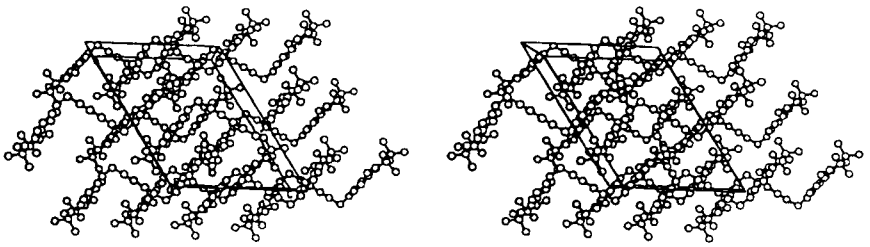

Figure 2. Stereoview of the packing pattern of diradical **1**, projected on the *ac* crystallographic plane.

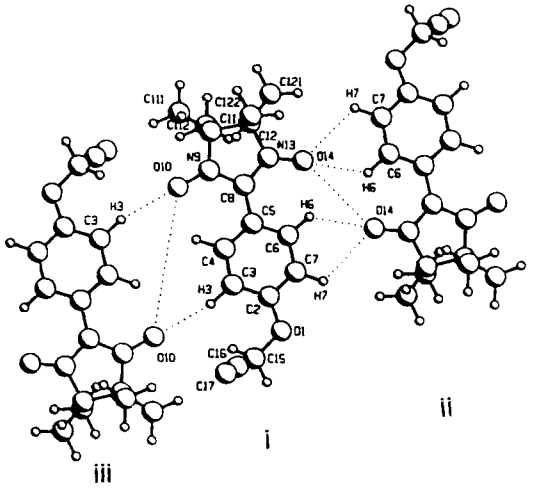

Figure 3. Projection of the crystal structure of diradical **1** on the plane defined by the atoms N9, C8, N13. The picture shows three adjacent radical centers within a stack. The short intermolecular contacts are indicated with broken lines. Symmetry codes: (*i*) x, y, z; (*ii*) $1.5 - x, 0.5 - y, -z$; (*iii*) $2 - x, -y, 1 - z$.

Table 3. Intermolecular Short Contacts in the Crystal Structure of Diradical 1[a]

contact	H···O	C···O	C−H···O[c]	O···O
C7−H7$^{(i)}$···O14$^{(ii)}$	2.866 Å	3.492 Å	117	
C6−H6$^{(i)}$···O14$^{(ii)}$	2.558 Å	3.347 Å	129	
C3−H3$^{(i)}$···O10$^{(iii)}$	2.397 Å	3.442 Å	163	
C4−H4$^{(i)}$···O10$^{(iii)}$	3.930 Å	4.170 Å	92	
O14$^{(i)}$···O14$^{(ii)}$				3.836 Å[b]
O10$^{(i)}$···O10$^{(iii)}$				5.666 Å[b]

[a] Symmetry code: (*i*) x, y, z; (*ii*) $1.5 - x, 0.5 - y, -z$; (*iii*) $2 - x, -y, 1 - z$. [b] Although on the basis of the adopted criterion this contact cannot be classified as a short one, it has been included in this table because it is useful for the presented magneto-structural correlation. [c] Angles in degrees.

in the solid state, predicted from its crystal structure, the effect of both radiation and heat on crystalline diradical **1** samples were studied. As initially expected, the crystals subjected to UV irradiation for 5 h at room temperature showed no noticeable changes either in their external appearance or in their IR and UV−visible spectra. A longer exposure to the radiation source (24 h) brought about the same results. However, a completely different result was obtained by thermal treatment of crystals of **1**. Thus, by heating at 90 °C in the dark, the initially deep blue color of crystals was gradually transformed into dark brown. A detailed examination showed that the crystal faces have developed hollows and had a wrinkled appearance. In addition, the samples subjected to thermal treatment display a reduced solubility in most of organic solvents, being only partially soluble in methanol, ethanol, and dimethylformamide, giving yellow solutions with such polar solvents. These results point out that the diradical **1** in this crystalline phase suffers by thermal treatment a real chemical reaction instead of a crystal-phase transition or a polymerization, as Zhang et al. wrongly claimed.[8] To discern the nature of the thermal process as well as to characterize the resulting reaction product(s), a detailed study has been performed and is set forth in the following.

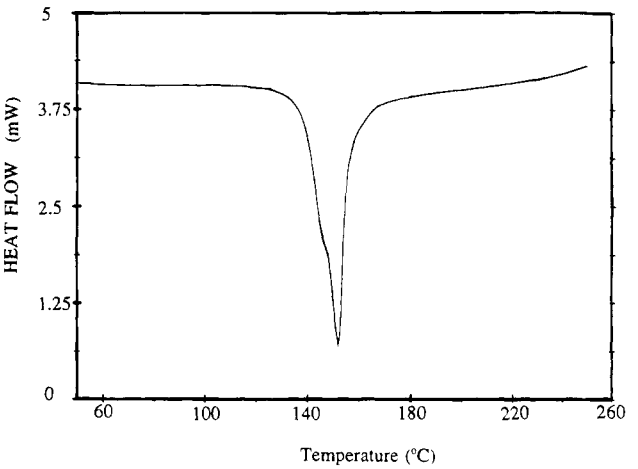

Figure 4. Exothermic DSC curve obtained for a polycrystalline sample of diradical **1**. Heating rate 1 °C min^{-1}; sample weight 1.804 mg; flow rate of Ar 40 cm^3 min^{-1}.

The thermal behavior of **1** has been studied both with differential scanning calorimetry (DSC) and with thermal gravimetric analysis (TGA) techniques. Dynamic DSC under Ar atmosphere at a heating rate of 1 °C min^{-1} (Figure 4) shows the onset of an exothermic process at 120 °C which peaks at around 150 °C and is essentially complete at 180 °C. The total enthalpy change for this process amounts to −175 kcal mol^{-1}. This value can be compared with the enthalpy usually evolved during the topochemical solid-state polymerizations of substituted diacetylenic monomers,[18] which is always in the range of 20−40 kcal mol^{-1}. These last experimental values are in fairly good accordance with the theoretically calculated one, 29.4 kcal mol^{-1}, taking into account only the structural reorganizations occurring in the diacetylenic units during the polymerization of DAs.[19] Although the higher exothermicity observed for the thermal reaction of diradical **1** does not preclude the solid-state polymerization of the diacetylenic moieties, it strongly suggests the occurrence of an additional

(18) (a) Bertault, M.; Schott, M.; Brienne, M. J.; Collet, A. *Chem. Phys.* **1984**, *85*, 481. (b) McGhie, A. R.; Lipscomb, G. F.; Garito, A. F.; Desai, K. N.; Kalyanaraman, P. S. *Makromol. Chem.* **1981**, *182*, 965. (c) Eckhardt, E.; Prusik, T.; Chance, R. R. In *Polydiacetylenes*; Bloor, D., Chance, R. R., Eds.; NATO ASI, Ser. E, No. 102; Martinus Nijhoff Publishers: Dordrecht, 1985; pp 25−39. (d) Patel, G. N. *Macromolecules* **1981**, *14*, 1170. (e) Bertault, J.; Canceill, M.; Collet, A.; Toupet, L. *J. Chem. Soc., Chem. Commun.* **1988**, 163.

(19) Patel, G. N.; Chance, R. R.; Turi, E. A.; Khanna, Y. P. *J. Am. Chem. Soc.* **1978**, *100*, 6644.

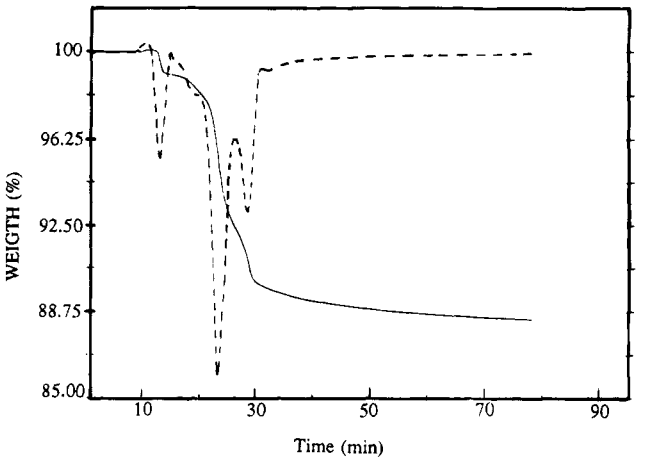

Figure 5. TGA curve for a polycrystalline sample (5.658 mg) of diradical **1** (solid line) and the first derivative of the TGA curve (dotted line). Temperature program: initial temperature, 50 °C; isothermal time 10 min; heating rate 15 °C min^{-1}; final temperature, 170 °C.

exothermal chemical reaction(s), in which breaking and formation of new covalent bonds occurs.[20] On the other hand, the first derivative of the DSC curve shows that the thermal reaction involves at least two overlapping exothermic processes (Figure 4), substantiating the complexity of the thermal process. Unfortunately by changing—within the range 0.1–5 °C min^{-1}—the rate of heating, no significant additional information was gained. Isothermal DSC curves recorded at temperatures comprised between 145 and 180 °C display the same characteristic features, but the two exothermic processes are somewhat more clearly resolved.

A further insight into the thermal behavior is obtained through the TGA technique. Figure 5 shows a typical curve recorded in isothermal regime at 170 °C under Ar. The two overlapping processes are now more clearly distinguished but not completely resolved, affording an overall weight loss of 10.5%. Finally, it is worth noting that under certain experimental conditions the thermal reaction of diradical **1** can proceed in an *explosive* fashion, specially when the sample weight is higher than 10 mg or when it is subjected to a steep heating rate; i.e., when the analyzed reaction system has not the proper heat drain that dissipates the large evolved enthalpy. A similar thermal behavior was previously reported for other diradical DAs.[5,6,20]

Characterization of Thermal Decomposition Products. The characterization of volatile products generated during the thermal reaction was carried out by using a mass spectrometer coupled to a gas chromatograph (GC-MS). With this technique only the solvent of the injected solution and gaseous NO were detected. Hence, the loss of two NO molecules by each diradical molecule and, therefore, the concomitant destruction of the radical centers, could in principle explain the overall weight loss of 10.5% observed by TGA.

The study of the nonvolatile solid product(s) generated during the thermal reaction was performed with conventional spectroscopic techniques, such as IR, UV–vis, and EPR. As expected, in the IR spectra of **1**, after its thermal treatment, most of the peaks corresponding to the diradical **1** disappear or display only a very reduced intensity (Figure 6). Additionally, no new peaks assignable to conjugated C=C bonds, corresponding to a polymeric backbone formed during the thermal reaction, appear.

The solid-state UV–visible spectrum (KBr dispersed) of diradical **1** is typical of phenyl-substituted α-nitronyl nitroxide radicals,[10] whereas the spectrum of a thermal treated sample is very different (Figure 7). In addition to the disappearance of the bands assigned to the radical centers, this thermally treated sample does not show

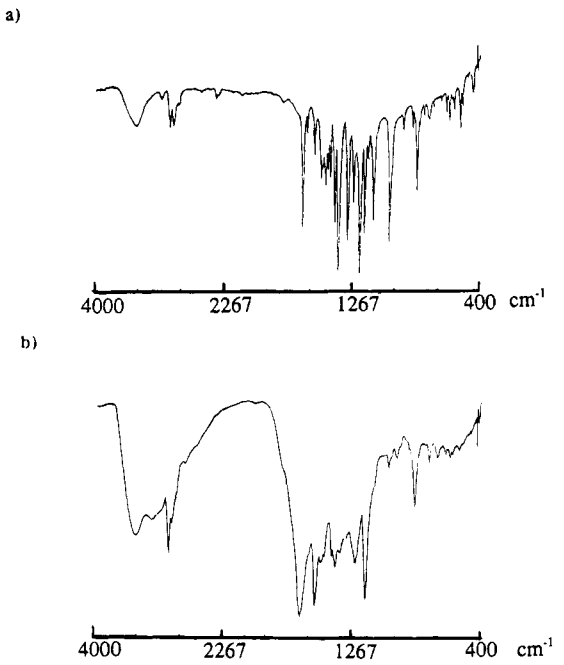

Figure 6. IR spectra of solid samples dispersed in KBr of (a) polycrystalline diradical **1** and (b) diradical **1** subjected to a thermal treatment at the TGA conditions under Ar.

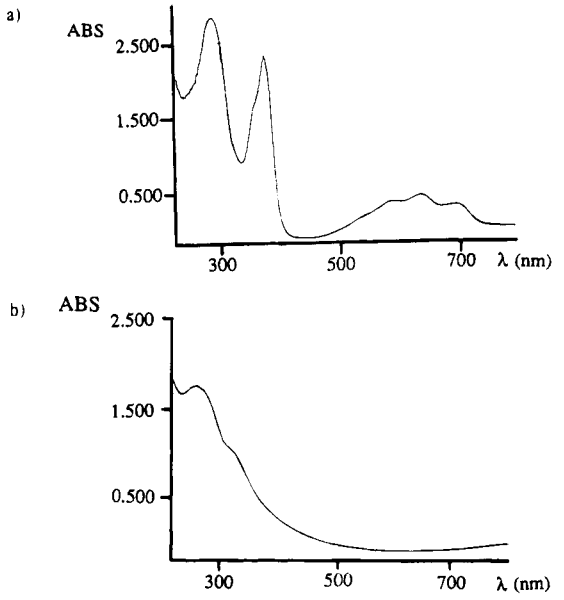

Figure 7. UV–visible spectra of solid samples dispersed in KBr of (a) polycrystalline diradical **1** and (b) diradical **1** subjected to a thermal treatment at the TGA conditions under Ar.

(20) (a) Inoue, K.; Koga, N.; Iwamura, H. *J. Am. Chem. Soc.* **1991**, *113*, 9803. (b) Iwamura, H.; Sasaki, S.; Sasagawa, N.; Inoue, K.; Koga, N. In *Magnetic Molecular Materials*; Gatteschi, D., Kahn, O., Miller, J. S., Palacio, F., Eds.; Kluwer Academic Publishers: Dordrecht, 1991; pp 53–66.

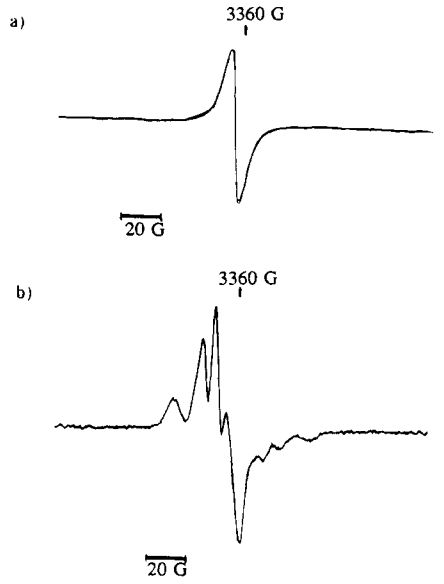

Figure 8. EPR spectra at room temperature of solid samples of (a) polycrystalline diradical **1** and (b) diradical **1** subjected to a thermal treatment in a sealed quartz tube filled with Ar.

any significative absorption between 500 and 650 nm—the spectral region in which the absorptions typical of polyconjugated polydiacetylene backbones are usually observed.[21]

The loss of radical centers in the thermally treated samples of diradical **1** was also confirmed from the magnetic properties. In fact, while the EPR spectrum of a polycrystalline sample of diradical **1** (Figure 8a) consists of an unique exchange narrowed Lorentzian line (vide infra), when this diradical is subjected to a thermal treatment, either under the TGA conditions or at 90 °C under Ar, it shows several dramatic changes in its EPR spectrum. Thus, together with a strong decrease of the total EPR signal intensity (ca. 70–90%) the appearance of a few new lines and the simultaneous broadening of such lines were observed (Figure 8b). All such spectral changes are in agreement with the picture that during the thermal treatment most of radicals centers are destroyed producing a magnetically diluted sample in which the exchange-narrowing mechanism turns inoperative. For such a reason the lines are broadened and the anisotropic g and hyperfine structures of the remaining isolated α-nitronyl nitroxide radical centers are apparent. Supporting this conclusion is the resemblance of the resulting spectrum with that obtained for a very diluted solution of diradical **1**, in frozen toluene at 150 K (see *Electron Paramagnetic Resonance Section*). On the other hand, the magnetic susceptibility measurements, performed between 10 and 200 K, confirm the above described picture. Actually, the paramagnetic susceptibilities of the polycrystalline diradical **1** and the thermally treated sample can be fitted to the Curie–Weiss law from which magnetic concentrations of 2.0×10^{21} and 3.1×10^{20} spins g^{-1}, respectively, are estimated, indicating that around the 85% of the spins initially present in the diradical sample are destroyed during the thermal treatment.

From the experimental studies reported so far it is concluded that *the thermal treatment of crystalline samples of diradical* **1** *brings about the loss of most of the radical centers in the sample.* The mechanism of the decomposition process is difficult to establish, but it involves the evolution of gaseous NO and, therefore, the destruction and rearrangement of the five-membered heterocyclic rings of the diradical structure. The formation of some polymer during the thermal reaction cannot be totally precluded from these studies. However, on the basis of the spectroscopic evidences and solubility characteristics, the polymeric nature of the resulting solid products is very dubious. This is a nonunexpected result, since as was previously mentioned the crystal packing of the diacetylenic moieties is unfavorable for a solid-state topochemical polymerization.

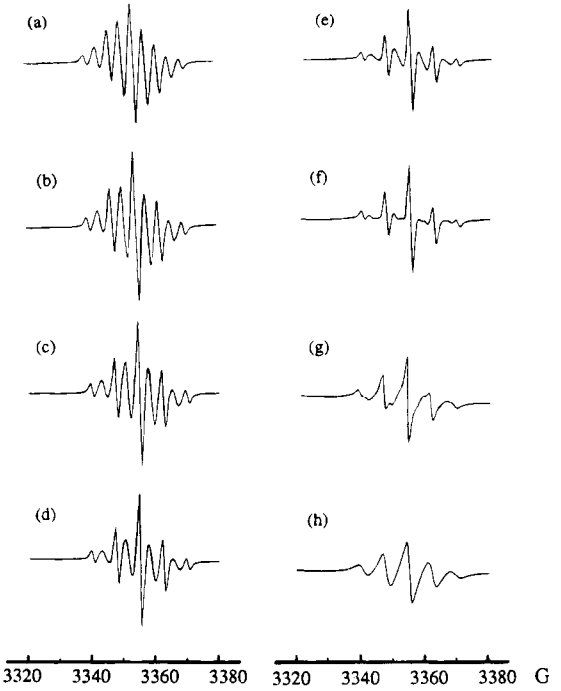

Figure 9. EPR spectra of pure diradical **1** in toluene solution at different temperatures: (a) 370, (b) 330, (c) 310, (d) 290, (e) 270, (f) 250, (g) 230, (h) 210 K. The vertical and horizontal scales are the same for all spectra.

Unfortunately, this is not the first time that attempts to obtain a high-spin polymers with a polydiacetylenic backbone and organic free radicals as side groups led to similar disappointing results. Actually, all assays directed toward the preparation of polyradical PDAs, having either nitroxide or triphenylmethyl radicals as side groups, have led either to the destruction of the radical moieties, during the thermal or radiative treatment, or to the lack of solid-state polymerizability of the involved monomers.[1a,20,22]

Electron Paramagnetic Resonance. *(a) Solution.* EPR experiments with dilute deoxygenated toluene solutions (ca. 10^{-3}–10^{-5} M) of diradical **1** provide a valuable insight into the *intramolecular exchange interaction* in this diradical (Figure 9).[23] At 210 K, the EPR spectrum consists of five relatively broad lines,

(21) (a) Wenz, G.; Müller, M. A.; Schmidt, M.; Wegner, G. *Macromolecules* **1984**, *17*, 837. (b) Matsuda, H.; Nakanishi, H.; Hosomi, T.; Kato, M. *Macromolecules* **1981**, *21*, 1238.

(22) (a) Wiley, D. W.; Calabrese, J. C.; Harlow, R. L.; Miller, J. S. *Angew. Chem., Int. Ed. Engl.* **1991**, *30*, 450. (b) Miller, J. S.; Glatzhofer, D. T.; Laversanne, R.; Brill, T. B.; Timken, M. D.; O'Connor, C. J.; Zhang, J. H.; Calabrese, J. C.; Epstein, A. J.; Chittipeddi, S.; Vaca, P. *Chem. Mater.* **1990**, *2*, 60.

(23) The low concentration in all these experiments precludes any possibility of *intermolecular exchange interactions*.

centered at $g_{iso} = 2.0060(1)$, with relative intensities of 1:2:3:2:1 and a constant splitting of 0.74 mT. This is the typical spectrum for substituted 2-phenyl α-nitronyl nitroxide monoradicals in which the electron spin is coupled with the ^{14}N nuclear spin of two equivalent nitrogen atoms with a hyperfine coupling constant, a_N, of 0.77(5) mT.[10,24] Therefore, this result suggests that at this temperature the two radical moieties of this compound behave magnetically independent at the EPR time scale, and hence the *intramolecular exchange coupling constant* between the two electron spins at each end of the diradical molecule, J^{intra}, is much smaller than the hyperfine coupling constant with the ^{14}N nuclear spins; i.e., the experimental spectrum at 210 K approaches to the *slow exchange limit* in which $J^{intra}/g\beta \ll a_N$ ($J^{intra}/hc \ll 10^{-3}$ cm^{-1}). With an increase of the temperature, four new groups of overlapping lines emerge among the initial five lines and at the same time two other groups of very weak overlapping lines appear beside the outermost of the initial five lines, giving rise to an extremely complex spectrum in which the lines alternate in line width and intensity, as, for example, is observed in the spectrum of 290 K (Figure 9). As the temperature is further increased, the intensities of the emerging four groups of lines increases and the two extreme groups of lines completely disappear, as is also shown in the Figure 9. Finally, at 370 K a nine-line EPR pattern with relative intensities approaching to 1:4:10:16:19:16:10:4:1 is observed. Such nine-line patterns have a nonconstant splitting that ranges between 0.37 and 0.39 mT; i.e., around one-half of the hyperfine splitting observed at 210 K. Therefore, this spectrum is close to the limiting case in which the two electron spins of the diradical molecule are strongly interacting at the EPR time scale being both electron spins coupled simultaneously with four equivalent nitrogen atoms; i.e., the experimental spectrum observed at 370 K approaches the *fast exchange limit* in which $J^{intra}/g\beta \gg a_N$.[25]

By analogy with the behavior of some nitroxide diradicals that show thermally activated weak intramolecular exchange interactions of this magnitude,[22b,26,27] the temperature dependence of EPR spectra observed for diradical **1** (Figure 9) could be ascribed to a time-dependent modulation of the intramolecular exchange coupling.[26] To confirm such a modulation, a theoretical model that permits us to determine the energies and transition probabilities for the allowed EPR-induced transitions of a system having the same structural and electronic characteristics of diradical **1** has been developed (see Appendix). As can be clearly seen from the results obtained with this theoretical model (see Figure 10), the temperature dependence of the EPR spectrum of the diradical is fully compatible with the evolution of the positions and relative intensities of the EPR lines predicted by the model due to the time-dependent modulation of the J^{intra} constant. In fact, the position of lines are perfectly simulated with this theoretical model, although in order to fit exactly the intensity and shape of the lines it will be necessary to introduce time-dependent line-width modulations; an objective that is outside the scope of the present work.

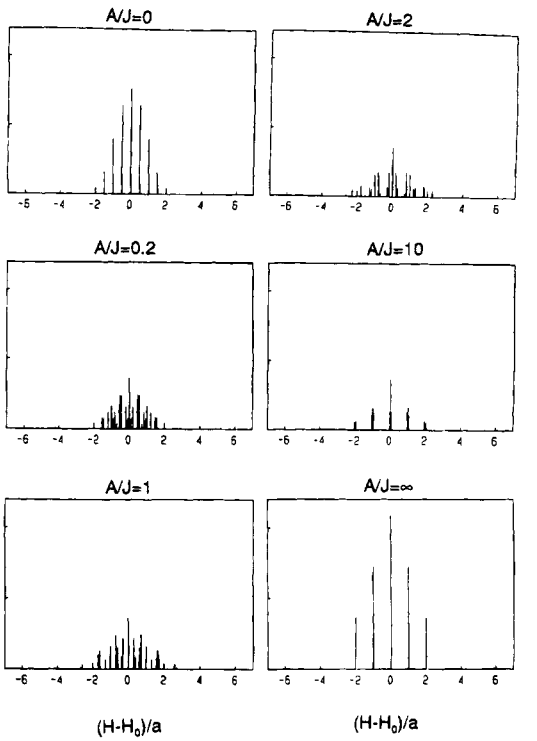

Figure 10. Stick plot diagrams of the EPR transition fields as a function of A_0/J^{intra} for a tumbling symmetrical diradical with a variable intramolecular exchange interaction having four equivalent nuclei with $I = 1$. The height of the sticks are proportional to the relative intensities of the EPR transitions.

At this point it must be emphasized that although this kind of time-dependent behavior has been previously observed and completely explained on a theoretical basis for some nitroxide diradicals,[22,26,27] to our knowledge this is the first time that it is observed in a α-nitronyl nitroxide diradical. Several mechanisms have been invoked to explain the origin of this behavior in unconjugated nitroxide diradicals:[26h] (1) an indirect exchange interaction via the spin polarization of the σ-bond electrons joining the two radical moieties, (2) an indirect exchange pathway involving the solvent molecules surrounding the radical centers, and (3) a through-space spin−spin interaction produced by thermally activated encounters of the two radical moieties of each molecule. The observed temperature dependence of J^{intra}, as well as the *slow exchange limit* observed for the spectrum at 210 K, are not consistent with the mechanism (1), since this mechanism must be always operative irrespective of the temperature. On the other hand, the room-temperature EPR spectrum of a toluene solution of the monoradical **2**, at the same concentration of radical centers as used in the spectrum of diradical **1**

(24) (a) Kreilick, R. W.; Becher, J.; Ullman, E. F. *J. Am. Chem. Soc.* **1969**, *91*, 5121−5124. (b) D'Anna, J. A.; Wharton, J. H. *J. Chem. Phys.* **1970**, *53*, 4047. (c) Davis, M. S.; Morokuma, K.; Kreilick, R. W. *J. Am. Chem. Soc.* **1972**, *94*, 5588−5592.

(25) Salem, L.; Rowland, C. *Angew. Chem., Int. Ed. Engl.* **1972**, *11*, 92−111.

(26) (a) McConnell, H. M. *J. Chem. Phys.* **1960**, *33*, 115. (b) Reitz, D. C.; Weissman, S. I. *J. Chem. Phys.* **1960**, *33*, 700. (c) Luckhurst, G. R. *Mol. Phys.* **1966**, *10*, 543. (d) Glarum, S. H.; Marshall, J. H. *J. Chem. Phys.* **1967**, *47*, 1374. (e) Luckhurst, G. R.; Pedulli, G. F. *J. Am. Chem. Soc.* **1970**, *92*, 4738. (f) Luckhurst, G. R.; Pedulli, G. F. *Mol. Phys.* **1971**, *20*, 1043. (g) Parmon, V. N.; Zhidomirov, G. M. *Mol. Phys.* **1974**, *27*, 367. (h) Luckhurst, G. R. In *Spin Labeling: Theory and Applications*; Berliner, L. J., Ed.; Academic Press: New York, 1976; pp 133−181. (i) Bencini, A.; Gatteschi, D. *EPR of Exchange Coupled Systems*; Springer-Verlag: Berlin, 1990; pp 187−192.

(27) (a) Brière, R.; Dupeyre, R.-M.; Lemaire, H.; Murat, C.; Rassat, A. *Bull. Soc. Chim. Fr.* **1965**, 3290. (b) Lemaire, H.; Rassat, A.; Rey, P.; Luckhurst, G. R. *Mol. Phys.* **1968**, *14*, 441. (c) Lemaire, H.; Rassat, A.; Rey, P. *Bull. Soc. Chim. Fr.* **1968**, 886.

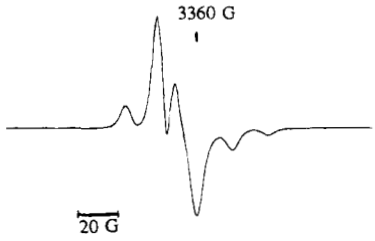

Figure 11. EPR spectra of randomly oriented molecules of diradical **1** in a frozen dilute toluene solution at 150 K. The vertical scale has been expanded relative to that of the spectra given in Figure 9.

(i.e., twice the molar concentration of the diradical), shows five sharp lines with relative intensities 1:2:3:2:1 and $a_N = 0.77$ mT. Thus, under the same experimental conditions (concentration and solvent), the molecules of monoradical **2**, which are similar to the two moieties of the diradical, do not exhibit any sign of magnetic exchange, therefore making unlikely the operativity of the mechanism mediated by solvent molecules. Consequently, the direct through-space interaction between the two radical centers at either end of the molecule remains as the most probable origin for the observed intramolecular magnetic exchange mechanism. Such a direct through-space interaction must be originated by a thermally activated flexing of the molecules and would account for the observed temperature dependence of the EPR spectrum of diradical **1**.[28] The suitability of this mechanism is supported by the high degree of flexibility of the molecular fragment joining the two radical moieties, in particular of the $-CH_2O-$ spacers. Thus, the spectrum obtained in the low-temperature limit (210 K) corresponds to the case in which the diradical molecule adopts a fixed conformation where $J^{intra}/g\beta \ll a_N$. From the measured a_N value, it is then possible to estimate an upper limit for the intramolecular exchange coupling constant of $J^{intra}/k \ll 0.001$ K (or $J^{intra}/hc \ll 10^{-3}$ cm^{-1}) for any fixed conformation of diradical **1**. Finally, as the temperature of the solution is decreased below the solvent freezing point, the EPR pattern is strongly modified (Figure 11). The spectrum is now typical of a rigid distribution of randomly oriented isolated α-nitronyl nitroxide radicals with a slightly anisotropic g constant and hyperfine interaction tensor.[24b] The anisotropies in the g and a_N tensors, which are apparent for orientations parallel and perpendicular to the molecular axes, are then responsible for the asymmetry of the resulting spectrum. The above result confirms therefore the magnetic isolation of the two radical moieties of **1** when this molecule adopts a rigid conformation.

(b) Solid State. As previously mentioned, the EPR spectrum of a polycrystalline sample of diradical **1** consists of only a single narrow Lorentzian line with $g_{av} = 2.0060(3)$ and $\Delta H_{pp} = 0.64$ mT. The integrated intensity of this signal varies as T^{-1}, in agreement with the temperature dependence of the static magnetic susceptibility. On the other hand, the ΔH_{pp} of the derivative spectrum as well as the line width at half-maximum intensity of the absorption spectrum, $\Delta H = 1.10$ mT, are temperature independent in the temperature range 150–300 K. The simplicity of the solid-state EPR spectrum of diradical **1** contrasts with the complexity already mentioned of the spectrum obtained with a diluted frozen solution; being, moreover, a clear indication about the presence of an *effective exchange-narrowing process* occurring in the condensed phase. In accord with the Anderson and Weiss relationship for exchange-narrowing processes[29] and with the extremely low magnitude estimated for the J^{intra} constant, the intradiradical origin of this narrowing process can be completely excluded. Therefore, the observed exchange-narrowing process must be ascribed to an *interdiradical interaction*, suggesting that the *intermolecular exchange coupling constant*, J^{inter}, must have a significative value; being the upper limit of this constant $J^{inter}/k \ll 150$ K. Consequently, the role that plays the diacetylenic unit in the diradical **1** is only structural and not electronic since it magnetically isolates the two radical centers of this molecule when it adopts a rigid and fixed conformation. Thus, it seems that this unit only acts as a structural spacer influencing the freedom of packing of the two radical moieties of the molecule, as already discussed.

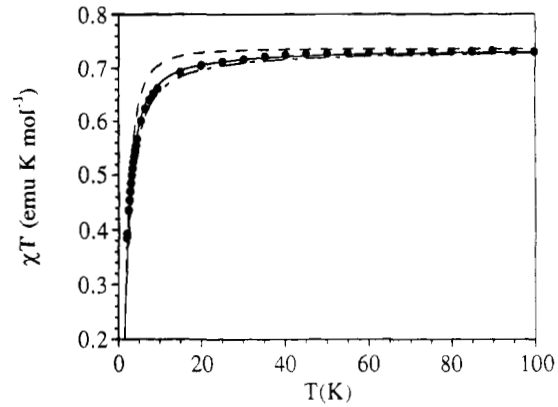

Figure 12. Magnetic behavior of a polycrystalline sample of diradical **1**. The solid line corresponds to the best fit to the F–AF alternating Heisenberg $S = 1/2$ chain model with $J_{AF}^{inter}/k = -3.9$ K, $\alpha = 0.3$, and $g = 2.006$. The behaviors for ideal cases with $\alpha = 0$ (i.e., the antiferromagnetic dimer) and $\alpha = 1$ are displayed as dashed lines.

Magnetic Susceptibility. The static magnetic susceptibility of a polycrystalline sample of **1** was measured by the SQUID method at an applied field of 0.1 T between 2 and 300 K. The temperature dependence of the product χT is reported in Figure 12. In the temperature range 100–300 K, the magnetic curve shows a relatively constant value of 0.73 emu K mol^{-1}, which corresponds to the theoretical value expected for two independent unpaired electrons per molecule with a g_{av} value of 2.006. A result which is in accordance with the negligible value of the J^{intra} constant and the estimated upper limit for the J^{inter} constant deduced from the EPR spectra. Below 25 K an abrupt decrease of χT is observed upon cooling, reaching a value of 0.39 emu K mol^{-1} at 2 K, in agreement with the presence of *dominant antiferromagnetic intermolecular interactions* in the crystal. In accordance with these facts, the experimental magnetic data can be fitted to the Curie–

(28) The existence of an intermolecular exchange coupling between radical centers in dilute toluene solution can be discarded on the basis of the fact that the EPR spectra recorded at room temperature in the concentration range 10^{-3}–10^{-5} M show no differences and, indeed, the spectrum obtained with the maximum dilution displays a nine-line pattern.

(29) Anderson, P. W.; Weiss, P. R. *Rev. Mod. Phys.* **1953**, *25*, 269.

Weiss law, with $C = 0.73$ emu K mol^{-1} and a negative θ value of ca. -2 K.[1a] Preliminary attempts to fit these experimental data to the Bleaney–Bowers equation for an antiferromagnetic dimer showed divergences mainly at low temperatures. In fact, the experimental data deviate downward such a theoretical curve, suggesting the simultaneous presence of very weak ferromagnetic interactions together with the dominant antiferromagnetic ones. Accordingly with this magnetic behavior, any sign of hysteresis, typical of a bulk ferromagnetic behavior, was observed in the magnetization curve measured at 2 K with an applied field in the range 0–5 T. This result is in total contradiction with that reported by Zhang et al.,[8] calling in question the validity of the result given by them, which probably could be ascribed to the uncertainty of the measuring equipment used.

To interpret the magnetic behavior of diradical **1**, we need first to examine in detail the intermolecular contacts in its crystalline structure. As we can see in Figure 3 the radical centers are stacked *side-by-side* and *heat-to-tail* along the two diagonals of the *bc* plane. In addition, there are no intermolecular distances shorter than 6 Å between any pair of atoms belonging to molecules in neighboring stacks. Therefore, according to this picture, it seems reasonable that the magnetic interactions between molecules belonging to neighboring stacks will be vanishingly small, so that the only relevant magnetic interactions in the crystal will be restricted to adjacent molecules within the stacks. On the other hand, the influence of the intramolecular magnetic interactions (between magnetic centers joined by the diacetylenic moiety and the spacers) on the macroscopic magnetic behavior of diradical **1**, can also be discarded with a high degree of confidence, based on the previously given EPR spectroscopic results and on structural considerations. In fact, the distances between the two nitronyl nitroxide moieties within a molecule are very large: d(O10···N9*) = 11.865 Å, d(O10···O10*) = 10.724 Å, d(O10···N13*) = 13.519 Å, d(O10···O14*) = 14.423 Å. Therefore, the resulting through-space intramolecular magnetic interactions, which depend on the direct overlap of the magnetic orbitals, are expected to be negligible. Finally, due to the lack of a π conjugation between the two radical moieties within the molecular backbone, a through-bond exchange mechanism can also be rejected in the analyses of the magnetic properties.

The analysis of the magnetic interactions between adjacent radical centers within the stacks has been accomplished in a qualitative fashion through the so-called *charge-transfer mechanism involving the frontier orbitals*.[30] The frontier orbitals that play the most relevant role in this mechanism are the SOMO (singly occupied molecular orbital), NHOMO (next highest doubly occupied molecular orbital), and LUMO (lowest unoccupied molecular orbital). The basic idea behind this mechanism is that a parallel spin alignment, or a ferromagnetic interaction, between two open-shell centers can arise from a configurational mixing between the ground electronic configuration and excited charge-transfer configurations. A SOMO–SOMO charge transfer will stabilize the low-spin state, favoring the antiferromagnetic interactions, while both NHOMO–SOMO and SOMO–LUMO charge transfers will preferentially stabilize the high-spin state, favoring therefore the ferromagnetic interactions. However, the stabilization of the high-spin state due to NHOMO–SOMO and SOMO–LUMO charge transfers is always 1 order of magnitude smaller than the stabilization of the low-spin state by SOMO–SOMO charge transfer. Under these circumstances, only when the overlap between SOMOs of the two neighboring radical centers is negligible may the overall magnetic interaction be ferromagnetic.[30] This mechanism was first employed to explain the presence of short-range intermolecular ferromagnetic interactions in crystals of the organic radical galvinoxyl and has been subsequently invoked in the interpretation of the relevant magnetic properties of several crystal phases of substituted 2-phenyl-α-nitronyl nitroxides.[13c–h,31,32] On the basis of this mechanism, the exchange interaction between the *i* and *iii* symmetry-related radical centers of diradical **1** (see Figure 3) is predicted to be ferromagnetic: the only short intermolecular contact, C3···O10, bears an NHOMO–SOMO and/or SOMO–LUMO orbital overlap.[33] It is worth noting that due to the large separation between the two nitronyl nitroxide moieties, d(O10···O10) = 5.666 Å, the SOMO–SOMO overlap can be reasonably neglected. The situation is reversed in the case of the *i* and *ii* symmetry-related radical centers of **1**. Despite the existence of similar NHOMO–SOMO and/or SOMO–LUMO overlaps, as revealed by short intermolecular contacts C6···O14 and C7···O14, in this case there exists a nonnegligibly small SOMO–SOMO overlap due to the short contact d(O14···O14) = 3.836 Å. This orbital overlap pattern satisfies the requirements for antiferromagnetic interactions to be dominant (vide supra).

Consequently, *the alternation in the characteristics of the intermolecular contacts, along the stacks of the radical side groups of diradical* ***1****, brings about an alternation of ferromagnetic (F) and antiferromagnetic (AF) intermolecular exchange interactions.*

From the magnetic point of view this situation may be quantitatively described in terms of a linear Heisenberg chain of $S = {}^1/_2$ spins with alternating F–AF intermolecular exchange interactions: $\cdots-J_F^{inter}-J_{AF}^{inter}-J_F^{inter}-J_{AF}^{inter}-\cdots J$. Therefore, the numerical approach recently developed by Borrás et al. for a $S = {}^1/_2$ Heisenberg chain with alternating ferromagnetic and antiferromagnetic interactions could be used to analyze the magnetic properties of the title compound.[34] For this kind of chains the theory predicts a maximum in

(30) (a) Goodenough, J. B. *Magnetism and the Chemical Bond*; Interscience Publishers: New York, 1963; p 167. (b) Kollmar, C.; Kahn, O. *Acc. Chem. Res.* **1993**, *26*, 259.

(31) Awaga, K.; Sugano, T.; Kinoshita, M. *Chem. Phys. Lett.* **1987**, *141*, 540.

(32) (a) Awaga, K.; Maruyama, Y. *J. Chem. Phys.* **1989**, *91*, 2743. (b) Hernàndez, E.; Mas, M.; Molins, E.; Rovira, C.; Veciana, J. *Angew. Chem., Int. Ed. Engl.* **1993**, *22*, 882–884.

(33) Semiempirical molecular orbital calculations (MNDO and AM1 versions) were carried out by using MOPAC; version 5.0 (QCPE 581), J. J. P. Stewart, Department of Chemistry, University of Indiana. The input geometry was that determined from X-ray diffraction studies. The calculations with minimized geometries indicated that the SOMO is exclusively localized on the ONCNO agrupation, while both NHOMO and LUMO are more widely spread over the whole molecule, although their major contribution is located on the phenyl substituent. This different spatial localization of the frontier orbitals is typical of α-nitronyl nitroxide radicals with an aromatic substituent in the α position.

(34) Borrás-Almenar, J. J.; Coronado, E.; Curely, J.; Georges, R.; Gianduzzo, J. C. *Inorg. Chem.*, in press.

the χT vs T plot when the ferromagnetic interaction is the dominant one (i.e., when the alternating parameter, defined as $\alpha = J_F/|J_{AF}|$, is larger than 1). By contrast, an antiferromagnetic-like behavior, without any maximum, is predicted in the reverse situation; i.e., when the alternating α parameter is smaller than one (see Figure 2 of ref 34). Our system does exhibit this last behavior, indicating that antiferromagnetic interactions are stronger than the ferromagnetic ones. In fact, the fitting of the data to the polynomial expressions of α and $kT/|J_{AF}|$ proposed in ref 34 in order to reproduce the numerical results of χ leads to the following parameters: $J_{AF}^{inter}/k = -3.9$ K and $\alpha = 0.3$ (solid line in Figure 12). In the same figure we have also plotted the calculated curves for the dimer limit ($\alpha = 0$) and for $\alpha = 1$. As we can see, the magnetic behavior is very slightly sensitive to the exchange alternation parameter, so that the resulting α value and hence the J_F^{inter}/k value of +1.2 K calculated from the last one, can be taken only as approximate. In turn, J_{AF}^{inter}/k remains unchanged when α varies from 0 to 1, indicating that the fit provides an accurate value of this parameter.

In conclusion, the weak ferromagnetic couplings present in this crystalline phase seems to indicate that the diacetylenic unit in diradical **1** acts as an efficient crystalline engineering tool that obstructs the natural tendency of radical centers to interact antiferromagnetically, probably by limiting the degrees of freedom for the packing of the radical side groups. Thus, under favorable circumstances, as seems to be the case in diradical **1**, such an obstruction could yield to the appearance of ferromagnetic interactions.

Comparison with Other Organic Radicals Showing Ferro- and Antiferromagnetic Interactions. To finish with the magnetic study of diradical **1**, it may be of interest to compare this system with other related organic magnetic materials for which exist evidences about the coexistence of ferro- and antiferromagnetic exchange interactions.

To our knowledge, the first example of an organic compound with such a characteristic has been recently reported by Awaga et al.[13g] The compound is also a derivative of an α-nitronyl nitroxide radical: the hydrated $(BF_4)_{0.72}{\cdot}I_{0.28}{\cdot}(H_2O)_{0.17}$ salt of the *meta-N*-methylpyridinium α-nitronyl nitroxide radical **4**. This compound crystallizes forming a two-dimensional triangular lattice of radical pairs with very short intermolecular distances which justifies the presence of dominant ferromagnetic interactions. It is also observed in the crystalline structure that each ferromagnetic pair is surrounded by four other pairs that interact antiferromagnetically in such a way that a 2D honeycomb-like network of alternating F−AF intermolecular interactions is expected to occur. On the basis of these magneto-structural considerations, the magnetic behavior of this compound was first interpreted by Awaga et al., using a mean-field-corrected dimeric model, in terms of a strong ferromagnetic intradimer interaction (J_F/k = +24.0 K) and a rather weak antiferromagnetic interdimer interaction ($\theta = -1.6$ K).[13g,35] Although this model explains qualitatively the magnetic behavior, it shows significative deviations from the experimental data, especially at low temperatures. For this reason we have reinterpreted these data using the F−AF alternating Heisenberg $S = 1/2$ chain model, obtaining good agreement with the experimental data in the whole temperature range (Figure S1). With this model the following set of exchange parameters have been obtained: $J_F^{inter}/k = +15.0$ K and $J_{AF}^{inter}/k = -2.5$ K ($\alpha = 6$), using a value of 2.010 for the g factor. The good agreement between the experimental magnetic data and the 1D model we used indicates that the magnetic behavior for this kind of system is almost insensitive to the dimensionality. In fact, the ground spin state of this 2D network is nonmagnetic ($S = 0$) as in the 1D case, and furthermore both systems should exhibit a qualitatively similar behavior with a maximum in χT when the ferromagnetic interaction is the dominant one; the only relevant difference is expected to occur in the position of the maximum, which mostly depends on the magnitude of the antiferromagnetic exchange. Therefore, while the 1D model gives a reliable value for the ferromagnetic exchange, the reported value for the antiferromagnetic exchange can be taken only as approximate.

A second example of a compound having opposed magnetic interactions has been reported by Iwamura et al.[36] These authors characterized the series of isomeric vinylidene derivatives of bis(*tert*-butyl nitroxide) diradicals **5**. For the *p,p'*-**5** diradical isomer, a rounded maximum in the χT vs T plot around 15 K is observed. As already mentioned, this behavior is characteristic of a F−AF alternating system with dominant ferromagnetic interactions. In fact, the mean-field corrected dimer model, used by Iwamura et al., gave a ferromagnetic coupling between the two nitroxide radical moieties ($J_F^{intra}/k = +15.3$ K) of the diradical and a weak antiferromagnetic Weiss constant ($\theta = -2.0$ K) that can be ascribed to antiferromagnetic intermolecular interactions between neighbor diradicals.

As in the previous case, the F−AF alternating Heisenberg $S = 1/2$ chain model reproduces better the experimental data in all the whole temperature range than the mean-field-corrected dimer model. In this way we have obtained $J_F^{intra}/k = +11.2$ K and $J_{AF}^{inter}/k = -4.0$ K ($\alpha = 2.8$) by using $g_{av} = 2.010$ (Figure S2). Unfortunately, the crystalline structure of this diradical is not

(35) A better fit of the experimental data has been achieved more recently by the same authors, using a more realistic structural model and the same molecular-field approximation, with the following exchange parameters $J_F^{inter}/K = +22.6$ K and $J_{AF}^{inter}/k = -2.4$ K. See: Awaga, K.; Okuno, T.; Yamaguchi, A.; Hasegawa, M.; Inabe, T.; Maruyama, Y.; Wada, N. *Phys. Rev. B* **1994**, *49*, 3975.

(36) Matsumoto, T.; Koga, N.; Iwamura, H. *J. Am. Chem. Soc.* **1992**, *114*, 5448.

known and, therefore, is not possible at the present time to confirm by a proper magneto-structural correlation the intermolecular nature of the observed antiferromagnetic interactions.

Experimental Part

General Methods. EPR spectra were recorded on a Bruker ESP 300 E X-band spectrometer operating at 9.4 GHz and equipped with a field-frequency lock accessory, a built-in NMR gaussmeter, a variable-temperature accessory, and a data acquisition system. g values were determined by the usual procedure using the gaussimeter or using a T_{104} dual sample with DPPH as standard. All precautions were taken to avoid undesirable spectral line broadening such as that arising from microwave power saturation and magnetic field overmodulation. To avoid dipolar broadening, the radical solutions used in the experiments were highly diluted and degassed, either by bubbling with pure argon or by using the freeze (liquid N_2)–pump–thaw (dry ice/acetone) technique, finally sealing the tubes under prepurified dry argon atmosphere. The ^{1}H NMR spectra were taken on a Bruker WP 80 SY instrument. Chemical shifts values were measured using the tetramethylsilane as an internal standard. UV–vis and IR spectra were measured on a Varian NIR–UV–vis Cary 5 and a Nicolet FT-IR 710 spectrometers, respectively. Magnetic susceptibility measurements were performed with a Quantum Design SQUID magnetometer at an applied field of 1.0 T between 2 and 300 K. The plastic sample holder was suspended from a cotton thread. The diamagnetic contributions to the total measured magnetic susceptibility was determined from the χT vs T plot in the high-temperature range. The UV irradiation of crystalline samples of diacetylenic diradical **1** was carried out with a mercury pressure arc lamp TQ-150 (spectral range 200–600 nm). The temperature of the sample was kept below 40 °C during the irradiation by using an external refrigeration. Thermal treatment of **1** for IR, UV–visible, and magnetic susceptibility studies was performed under TGA conditions in Ar. Variable quantities of the material (5–10 mg) were placed in a SiO_2 pan and subjected to isothermal treatment at 170 °C. Samples for EPR studies were prepared in an EPR quartz tube under N_2 atmosphere and placed in a heating bath with temperature controller at 95 °C for 24 h. The handling of the samples before and after the thermal treatment was performed with Teflon-coated utensils to avoid metallic impurities. Thermal analyses were performed using a Perkin-Elmer DSC-7 differential scanning calorimeter and a Perkin-Elmer TGA-7 thermogravimetric analyzer. Mass spectra were recorded on a VG TS-250 spectrometer with DEI ionization (70 eV). The characterization of volatile products generated during the thermal reaction of diradical **1** was carried out by using the same mass spectrometer coupled to a Shimadzu GC-15A gas chromatograph. In these experiments a saturated chloroform solution of diradical **1** was injected into the chromatograph and the temperature of the injector was allowed to raise continuously from room temperature, at a heating rate of 5 °C min^{-1}; while the ions generated from the resulting volatile decomposition products were detected with the mass spectrometer. No product different from chloroform was detected until the GC injector reach to 160 °C. At this temperature, only a single peak at m/z = 30, attributed to gaseous NO, was detected. Melting points were obtained with a Köfler microscope and are uncorrected. Microanalyses were performed at the Microanalysis Service of the Centre d'Investigació i Desenvolupament of Barcelona (CSIC). Reagents and solvents were obtained commercially and used without further purification unless otherwise noted. THF was distilled from benzophenone ketyl under argon immediately before use. The handling of radicals in solution was performed under red light or in the dark.

Preparation of the Radical 2-[4-(2-Propynyloxy)phenyl)]-4,4,5,5-tetramethyl-4,5-dihydro-1*H*-imidazole-1-oxyl 3-*N*-Oxide (2). In a dried, argon-filled, round-bottomed flask, fitted with a magnetic stirrer and an addition funnel, radical phenol **3**[10,32b] (0.35 g, 1.47 mmol) and potassium *tert*-butoxide (0.17 g, 1.55 mmol) were dissolved in THF (15 mL). The resulting solution was cooled in an ice-water bath at 0 °C and a solution of 2-propynyl *p*-toluenesulfonate (0.20 g, 0.90 mmol) in THF (15 mL) was added dropwise. The mixture was stirred and heated in an oil bath at 70–75 °C for 20 h. The insoluble solid was then filtered off on a sintered-glass funnel and rinsed with THF (40 mL) and $CHCl_3$ (60 mL). The solvent was evaporated, and the crude product was chromatographed on a silica gel column (45 × 3 cm, 230–400 mesh) using ethyl acetate–chloroform (1:1) as eluent, yielding a deep blue solid which recrystallized from carbon tetrachloride as blue needles of **2** (0.24 g, 66%); mp 187–9 °C (with decomposition). IR (KBr) γ 3212, 2123, 1604, 1493, 1385, 1364, 1252, 1135 cm^{-1}. UV–vis (THF) λ 280, 366, 627 nm (log ϵ 4.2, 4.1, 3.2). EPR ($CHCl_3$) g = 2.0060, a_N = 0.77 mT, ΔH_{pp} = 0.13 mT. MS(EI) m/z (%), 287 (M^+, 41.5), 84 (100). Anal. Calcd for $C_{16}H_{19}N_2O_3$: C, 66.88; H, 6.66; N, 9.75%. Found: C, 66.96; H, 6.69; N, 9.74%.

Preparation of the Diradical 2,4-Hexadiynylenedioxy Bis[2-(*p*-phenylene)-4,4,5,5-tetramethyl-4,5-dihydro-1*H*-imidazole-1-oxy 3-*N*-oxide] (1). A mixture of finely powdered copper(I) chloride (0.02 g, 0.25 mmol) and *N,N,N',N'*-tetramethylethylenediamine (0.06 g, 0.50 mmol) in $CHCl_3$ (5 mL) was vigorously shaken under O_2 at room temperature for 15 min, and then a solution of radical **2** (0.28 g, 1 mmol) in $CHCl_3$ (5 mL) was added, and the system was vigorously shaken under O_2 at room temperature for 24 h. The solvent was evaporated, and the crude product was chromatographed on a silica gel column (45 × 3 cm, 230–400 mesh) using ethyl acetate–chloroform (4:1) as eluent, affording a deep blue solid which recrystallized from chloroform giving the diradical **1** as blue flat plates (0.26 g, 90%). IR (KBr) γ 2147, 1605, 1487, 1389, 1362, 1303, 1237, 1217, 1134, 1019 cm^{-1}. UV–vis (THF) ϵ, 281, 366, 627 nm (log ϵ 4.6, 4.4, 3.1), MS (EI); m/z (%) 84 (100). Anal. Calcd for $C_{32}H_{36}N_4O_6$: C, 67.12; H, 6.34; N, 9.78%. Found: C, 66.85; H, 6.38; N, 9.59%.

X-ray Data Collection and Structure Determination.[37] A blue prismatic crystal having approximate dimensions of 0.63 × 0.51 × 0.12 mm was used for the X-ray diffraction study. The experiment was performed on an Enraf-Nonius CAD4 diffractometer using Mo Kα radiation (λ = 0.710 73 Å). Cell constants and the orientation matrix were obtained from least-squares analysis of 25 high-angle reflections. The monoclinic cell parameters and the calculated cell volume are a = 16.57(2) Å, b = 16.116(2) Å, c = 13.10(1) Å, β = 123.05(4)°, V = 2931(4) Å^3. For Z = 4 and M_w = 572.67 the calculated density is 1.30 g cm^{-3}. The $C2/c$ space group was assumed according to the extinguished reflections. Data were collected at the temperature of 294 K using an ω–2θ scan up to a $2\theta_{max}$ of 50° and the hkl ranges were as follows: $-19 < h < 19$, $0 < k < 19$, and $0 < l < 15$. A total of 3232 reflections were collected from which 2984 were unique. Standard reflections decay was 0.9%. Lorentz and polarization corrections were applied to the data. The linear absorption coefficient is 0.8 cm^{-1} for the Mo Kα radiation. An empirical correction was applied to the data (relative transmission coefficients ranged from 0.904 to 0.999 with an average value of 0.941). Intensities of equivalent reflections were averaged with an agreement factor of 2.9% based on F_o. The structure was solved by direct methods.[38] A total of two phase sets were produced. The 21 non-hydrogen atoms were located from the E-map prepared from the phase set with an absolute figure of merit of 1.140, a residual of 15.10, and ψ_0 of 0.794. The hydrogen atoms were calculated, and their positions and thermal parameters were refined. The structure was refined in full-matrix least squares using 1272 reflections with $F > 1\sigma(F)$.[39] The final cycle of

(37) MOLEN, *An Interactive Structure Solution Procedure*; Enraf-Nonius: Delft, The Netherlands, 1990.

(38) Main, P.; Fiske, S. J.; Hull, S. E.; Lessinger, L.; Germain, G.; De Clerq, J. P.; Woolfson, M. M. MULTAN 80, *A System of Computer Programs for the Automatic Solution of Crystal Structures from X-Ray Diffraction Data*; University of York, England, 1980.

(39) Sheldrick, G. M., SHELX 76, *A Program for Crystal Structure Determination*; University of Cambridge, England, 1976.

refinement included 192 variable parameters and converged with an unweighted and weighted agreement factors of 0.092 and 0.116. The highest peak and the minimum negative peak in the final difference Fourier had heights of 0.399 and −0.253 e/Å^3, respectively.

Acknowledgment. This research was supported by the Programa Nacional de Nuevos Materiales, C.I.C.yT. (Grant MAT91-0553) and the Human Capital and Mobility Program of the European Union (Network on *Magnetic Molecular Materials*, Grant ERBCHRX-CT920080, and a Post Doctoral grant to J.J.B.-A.). We thank Prof. J. L. Serrano (Instituto de Ciencia de Materiales de Aragón, CSIC, Universidad de Zaragoza) for the GC-MS experiments and to Prof K. Awaga (The University of Tokyo) for providing us some data.

Supplementary Material Available: Magnetic behaviors of radicals **4** and **5**, selected bond lengths and angles, and anisotropic thermal parameters (5 pages); structure factors of diradical **1** (8 pages). Ordering information is given on any current masthead page.

Appendix. Theoretical EPR Absorption Lines for Tumbling Symmetrical Diradicals Having Four Equivalent Nuclei with $I = 1$ and a Modulated Electron-Exchange Interaction

Positions, line widths, and relative intensities of the multiple EPR lines showed by a tumbling diradical formed by the linkage of two molecular fragments, each containing one unpaired electron and one magnetically active nucleus, have been put on a quantitative basis using several theoretical models.[26] It is well-known that all the above-mentioned spectral features show a strong dependence on the strength of the electron-exchange coupling between the two fragments producing very characteristic and complex EPR line patterns. At first glance, such line patterns look like that previously described for diradical **1**, as well as for other diradicals having two magnetically active nuclei on each molecular fragment.[40] However the already existing theoretical models are not directly applicable in their present forms to describe the positions and relative intensities of the EPR lines for diradicals with such characteristics, since they are only applicable to systems with two equivalent $I = 1$ nuclei.[26] Hereupon, the correct equations to apply to diradicals with four equivalent $I = 1$ nuclei are readily demonstrated.

The Hamiltonian that describes the state energies and allowed transitions for a tumbling system formed by two molecular fragments, A and B, each containing one unpaired electron and several magnetically active nuclei is given by the following equation:[41]

$$\mathcal{H} = g_1\mu_B\mathbf{H}\cdot\mathbf{S}_{1z} + g_2\mu_B\mathbf{H}\cdot\mathbf{S}_{2z} + \sum_i A_i^{(A)}\mathbf{S}_1\cdot\mathbf{I}_i + \sum_j A_j^{(B)}\mathbf{S}_2\cdot\mathbf{I}_j + J\mathbf{S}_1\cdot\mathbf{S}_2 \quad (1)$$

in which the first two right-handed terms take into account the purely electronic Zeeman interactions, the third and fourth terms correspond to the hyperfine interactions between the electron spins and nuclear spins on both fragments, and the fifth term describes the exchange interaction between electron spins associated to each molecular fragment. In eq 1 g_i is the isotropic Landé factors associated with electrons 1 and 2, $\mathbf{S}_{1z}$ and $\mathbf{S}_{2z}$ are the z components of the corresponding electron spin operators, $\mathbf{I}_i$ is the nuclear spin operator of the active nucleus i, $A_i^{(x)}$ is the isotropic hyperfine coupling constant of the nucleus i belonging to the fragment x = A or B, $\mathbf{H}$ is the applied magnetic field, and J is the intramolecular exchange constant.

Assuming that hyperfine interactions are smaller than the purely electronic Zeeman interactions, the corresponding nonsecular hyperfine terms can be neglected and hence the system is well described by the effective Hamiltonian:

$$\mathcal{H}_{eff} = g_1^{eff}\mu_B\mathbf{H}\cdot\mathbf{S}_{1z} + g_2^{eff}\mu_B\mathbf{H}\cdot\mathbf{S}_{2z} + J\mathbf{S}_1\cdot\mathbf{S}_2 \quad (2)$$

in which the effective g factors are given by

$$g_1^{eff} = g_1 + (\mu_B H)^{-1}\sum_i A_i^{(x)} m_i^{(x)} \quad (3)$$

$$g_2^{eff} = g_2 + (\mu_B H)^{-1}\sum_j A_j^{(x)} m_j^{(x)} \quad (4)$$

with $m_i^{(x)}$ the nuclear quantum number of each nucleus i belonging to the molecular fragment x, with x = A or B.

The eigenvalues of the effective Hamiltonian $\mathcal{H}_{eff}$ are[42]

$$E_{|1,1\rangle} = +{}^1/_2(g_1^{eff} + g_2^{eff})\mu_B H + J/4 \quad (5)$$

$$E_{|0,+\rangle} = +{}^1/_2(g_1^{eff} - g_2^{eff})\mu_B H \tan\theta + J/4 \quad (6)$$

$$E_{|1,-1\rangle} = -{}^1/_2(g_1^{eff} + g_2^{eff})\mu_B H + J/4 \quad (7)$$

$$E_{|0,-\rangle} = -{}^1/_2(g_1^{eff} - g_2^{eff})\mu_B H \tan\theta - 3J/4 \quad (8)$$

with $\theta = {}^1/_2 \arctan[(g_1^{eff} - g_2^{eff})\mu_B H/J]$.

Then, for a general diradical case the allowed transitions, together with their corresponding energies, and

(40) (a) Cordes, A. W.; Haddon, R. C.; Oakley, R. T.; Schneemeyer, L. F.; Waszczak, J. V.; Young, K. M.; Zimmerman, N. M. *J. Am. Chem. Soc.* **1991**, *113*, 582. (b) Andrews, M. P.; Cordes, A. W.; Douglass, D. C.; Fleming, R. M.; Glarum, S. H.; Haddon, R. C.; Marsh, P.; Oakley, R. T.; Palstra, T. T. M.; Schneemeyer, L. F.; Trucks, G. W.; Tycko, R.; Waszczak, J. V.; Young, K. M.; Zimmerman, N. M. *J. Am. Chem. Soc.* **1991**, *113*, 3559.

(41) For a diradical in a solid one must also consider the electron spin−electron spin dipolar term, $\mathbf{S}_1\cdot\mathbf{D}\cdot\mathbf{S}_2$; however, since the trace of the **D** tensor is zero, the effects of this term average out in solution, providing the elements of **D** are small.

(42) The eigenfunctions of the effective Hamiltonian are $|1,1\rangle$, $|1,-1\rangle$, $|0,+\rangle = \cos\theta|1,0\rangle + \sin\theta|0,0\rangle$, and $|0,-\rangle = \sin\theta|1,0\rangle - \cos\theta|0,0\rangle$. The set of functions $|0,0\rangle$ and $|1,1\rangle$, $|1,0\rangle$, and $|1,-1\rangle$ are the classical eigenfunctions for a symmetrical diradical system with negligible hyperfine interactions; i.e., the functions describing the singlet state with $S = 0$ and $M_s = 0$ and the triplet state with $S = 1$ and $M_s = +1$, 0, and −1, respectively. See: Wertz, J. E.; Bolton, J. R. *Electron Spin Resonance. Elementary Theory and Practical Applications*; Chapman and Hall: New York, 1972; pp 223−256.

transition probabilities, P, are given by[43]

T_{+1} transition, $|0,+\rangle \leftrightarrow |1,1\rangle$

$$h\nu_0 = +{}^1/_2(g_1^{\text{eff}} + g_2^{\text{eff}})\mu_B H - {}^1/_2(g_1^{\text{eff}} - g_2^{\text{eff}})\mu_B H \tan\theta \quad (9a)$$

$$P = 1 + \cos 2\theta \quad (9b)$$

T_{-1} transition, $|0,+\rangle \leftrightarrow |1,-1\rangle$

$$h\nu_0 = +{}^1/_2(g_1^{\text{eff}} + g_2^{\text{eff}})\mu_B H + {}^1/_2(g_1^{\text{eff}} - g_2^{\text{eff}})\mu_B H \tan\theta \quad (10a)$$

$$P = 1 + \cos 2\theta \quad (10b)$$

S_{+1} transition, $|0,-\rangle \leftrightarrow |1,1\rangle$

$$h\nu_0 = +{}^1/_2(g_1^{\text{eff}} + g_2^{\text{eff}})\mu_B H + {}^1/_2(g_1^{\text{eff}} - g_2^{\text{eff}})\mu_B H \tan\theta + J \quad (11a)$$

$$P = 1 - \cos 2\theta \quad (11b)$$

S_{-1} transition, $|0,-\rangle \leftrightarrow |1,-1\rangle$

$$h\nu_0 = +{}^1/_2(g_1^{\text{eff}} + g_2^{\text{eff}})\mu_B H - {}^1/_2(g_1^{\text{eff}} - g_2^{\text{eff}})\mu_B H \tan\theta - J \quad (12a)$$

$$P = 1 - \cos 2\theta \quad (12b)$$

Equations 9–12 can be used to determine the resonance fields and relative intensities of the EPR lines corresponding to each transition that shows a tumbling symmetrical diradical with two equivalent magnetically active nuclei on each molecular fragment; i.e., with $g_1 = g_2 = g$ and $A_i^{(x)} = A_i^{(x)} = A_0$; $i = j = 1, 2$ and $x =$ A or B. Such spectral features in a compact form are given by

$$H_{T\pm1} = H_0 - aM_I/2 \pm a\Delta M_I(\tan\theta)/2 \quad (13a)$$

$$P_{T\pm1} = 1 + \cos 2\theta \quad (13b)$$

$$H_{S\pm1} = H_0 - aM_I/2 \mp a\Delta M_I(\tan\theta)/2 \mp aJ/A_0 \quad (14a)$$

$$P_{S\pm1} = 1 - \cos 2\theta \quad (14b)$$

where $H_0 = h\nu_0/g\mu_B$, $a = A_0/g\mu_B$, $M_I = m_1^{(A)} + m_2^{(A)} + m_1^{(B)} + m_2^{(B)}$, $\Delta M_I = [m_1^{(A)} + m_2^{(A)}] - [m_1^{(B)} + m_2^{(B)}]$, and $\theta = \arctan(\Delta M_I A_0/J)$. Therefore, for a diradical having two equivalent ^{14}N atoms with $I = 1$ on each molecular fragment, as occurs in the diacetylenic diradical **1**, one would expect to find a maximum of 286 lines according to the different combinations of $m_i^{(x)}$ values for the four magnetically active nuclei of the molecule. Depending on the A_0/J ratio, some of the lines must be degenerated and the relative intensities of the other of those lines must be negligible, since they turn forbidden ($P = 0$); producing an extremely complex EPR line pattern which will be characteristic of the A_0/J ratio.[44] In Figure 10 stick diagrams showing the transition fields and the relative intensities for various values of the A_0/J ratio are presented. Thus, for values of $A_0/J \rightarrow \infty$ the spectra must show five lines separated by a constant a value and with an intensity ratio of 1:2:3:2:1. This situation corresponds to the interaction of each unpaired electron of the diradical with only two ^{14}N atoms; i.e., it corresponds to the *slow exchange limit*. When $A_0/J \rightarrow 0$, the spectrum consists of nine lines equally spaced by a value of $a/2$ showing relative intensities of 1:4:10:16:19:16:10:4:1, as expected to occur in the *fast exchange limit*; i.e., for strongly coupled electrons that interact with all four ^{14}N atoms of the molecule. For intermediae A_0/J values, 286 transitions must be observed, 162 of them being of the $T_{\pm1}$ type and the 124 remaining of the $S_{\pm1}$ one. In this *intermediate exchange region*, it is convenient to describe and discuss all these lines grouped according to their associated ΔM_I values. Thus, for lines with $|\Delta M_I| = 1, 2, 3$, or 4 all the transitions, either those of $T_{\pm1}$ or $S_{\pm1}$ types, are allowed, each one appearing split at both sides of H_0; furthermore the $S_{\pm1}$ lines are separated from the other ones by roughly the exchange energy. So, for ratios of $A_0/J < 0.5$, all the $S_{\pm1}$ type transitions must lie outside the central region of the spectrum and with a decrease in A_0/J, the intensities of the $S_{\pm1}$ transitions will decrease until eventually disappearing and only the remaining $T_{\pm1}$ transitions will appear in the spectrum. On the other hand, for lines with $\Delta M_I = 0$ all the $S_{\pm1}$ transitions are forbidden, while those of the $T_{\pm1}$ type are all allowed, appearing degenerated in five positions with constant relative intensities. Thus, such lines will appear at the constant resonance fields of H_0, $H_0 \pm a$, and $H_0 \pm 2a$ and, therefore, they will present constant line widths regardless of the A_0/J value. Without any doubt, the last spectral features are the most remarkable ones in the present discussion since they are responsible for most of the main characteristics of the EPR line pattern showed by tumbling symmetrical diradicals with four equivalent $I = 1$ nuclei having a moderate exchange interaction which is modulated by some time-dependent perturbation. In such a type of diradicals the $T_{\pm1}$ transitions with $\Delta M_I = 0$ will remain unaffected by the modulation of J, while the transitions with values of $|\Delta M_I| = 1, 2, 3$, or 4 will be strongly influenced by this phenomenon. Thus in the so-called intermediate exchange region, by increasing the rate of the J modulation the five lines that appear at H_0, $H_0 \pm a$, and $H_0 \pm 2a$ will remain unaffected, while the rest of the transitions will appear at intermediate and extreme positions with respect to the above-mentioned five lines; those transitions appearing grouped, forming broad lines. When the fast exchange limit is approached, most of these changing lines coalesce at particular positions and start to narrow until they finally appear at the resonance fields of H_0, $H_0 \pm a/2$, $H_0 \pm a$, $H_0 \pm 3a/2$, and $H_0 \pm 2a$ like nine narrow lines.

(43) Transitions are labeled according to the states which are involved with. Thus, transitions involving the $|0,+\rangle$ state, which has a large triplet character (see ref 41) $|0,+\rangle$ state[41] for the cos $\theta \approx 1$ case) are labeled by $T_{\pm1}$; while transitions associated with the $|0,-\rangle$ state are labeled by $S_{\pm1}$ due to the higher singlet character of such a state.

(44) A complete EPR spectrum simulation would require taking into consideration the strikingly different line width of each line of the spectrum. This could be done by using either the density spin-matrix formalism or the Redfield theory, properly adapted to the present case. For extensive descriptions of such theories see: Parmon, V. N.; Zhidomirov, G. M. *Mol. Phys.* **1974**, *27*, 367. Luckhurst, G. R. *Mol. Phys.* **1966**, *10*, 543. Luckhurst, G. R.; Pedulli, G. F. *Mol. Phys.* **1971**, *20*, 1043. Luckhurst, G. R.; Pedulli, G. F. *J. Am. Chem. Soc.* **1970**, *92*, 4738.